Applied Energy 232 (2018) 443–450

Contents lists available at ScienceDirect

Applied Energy

journal homepage: www.elsevier.com/locate/apenergy

Two-phase flow in the mixed-wettability gas diffusion layer of proton exchange membrane fuel cells

Zhiqiang Niu[a,b], Zhiming Bao[a], Jingtian Wu[b], Yun Wang[b,*], Kui Jiao[a,*]

[a] State Key Laboratory of Engines, Tianjin University, 135 Yaguan Rd, Tianjin 300350, China
[b] Renewable Energy Resources Lab (RERL), Department of Mechanical and Aerospace Engineering, University of California, Irvine, CA 92697-3975, United States

HIGHLIGHTS

- Two-phase flow in mixed-wettability GDLs are investigated using a 3D VOF model.
- The GDL microstructures of PTFE spatial distribution are digitally reconstructed.
- The VOF predictions are compared with the LBM and experimental results.
- The effects of the PTFE distribution on water dynamics are studied.

ARTICLE INFO

Keywords:
Fuel cell
Gas diffusion layer
Mixed wettability
Capillary pressure
Volume of fluid
PTFE drying

ABSTRACT

Polytetrafluoroethylene (PTFE) is widely employed to improve the hydrophobicity of gas diffusion layer (GDL) in proton exchange membrane (PEM) fuel cells. In this study, the effects of different PTFE loadings on the relationship of the capillary pressure P_c and water saturation s in the mixed-wettability GDL, i.e. P_c-s, are investigated using a three-dimensional (3D) volume of fluid (VOF) model. The simulated P_c-s curves are presented and compared with results obtained from the lattice Boltzmann model (LBM) and experiments. The good agreement between the VOF predictions and experiment data is achieved, indicating that the mixed wettability in the PTFE treated GDL is an important feature to understand two-phase behaviors in fuel cells. The homogeneous and heterogeneous PTFE distributions resulted from two PTFE drying methods (i.e. the vacuum and air dryings, respectively) are studied. It was found that the air drying GDL yields a high PTFE concentration near the water inlet and reduces water imbibition near the inlet. The simulated P_c-s correlation from VOF model was compared with standard Leverett correlation.

1. Introduction

Proton exchange membrane (PEM) fuel cells are promising alternative power devices of electric vehicles due to their outstanding merits such as high efficiency, negligible emissions and high power density. Water management is a major bottleneck for the improvement of fuel cell efficiency and durability [1]. In PEM fuel cells, the gas diffusion layer (GDL) is a key component which provides pore paths for reactant diffusion and product water removal. Excessive liquid water in GDLs may hinder reactant transport and increases the mass transport polarization [2]. Thus, effective water removal is important to ensure high efficient operation of fuel cells [3]. This issue requires comprehensive understanding of liquid water transport in GDLs [4].

In general, GDLs are fibrous media, and carbon paper and carbon cloth are popular GDL materials [5,6], as shown in Fig. 1. The inherent hydrophilicity of graphite (its static contact angle $\theta \approx 75$–86° [7–9]) may resist water removal in GDLs. A common strategy of facilitating water removal is to add hydrophobic agents, such as Polytetrafluoroethylene (PTFE) [10–15]. In fabrication, it is difficult to coat PTFE homogeneously in all the inner surfaces, causing the treated GDL to show mixed wettability, i.e. the part of the GDL inner surface is hydrophobic, and the rest is hydrophilic. In addition, PTFE loadings (typically 5–30 wt%) [12,13], loss during mechanical compression or freezing cycles [14,15], degradation [16–19], and drying methods (e.g. air versus vacuum drying) [20] will impact the PTFE distribution and mixed wettability in GDLs.

Several experiments were conducted to assess the GDL's mixed wettability and measure the correlation between the capillary pressure P_c (defined as $P_c = P_l - P_g$) and water saturation s in GDLs [21–26]. Gostick et al. [21,22] employed the standard porosimetry (MSP)

* Corresponding authors.
E-mail addresses: yunw@uci.edu (Y. Wang), kjiao@tju.edu.cn (K. Jiao).

https://doi.org/10.1016/j.apenergy.2018.09.209
Received 15 May 2018; Received in revised form 24 September 2018; Accepted 25 September 2018
Available online 05 October 2018
0306-2619/

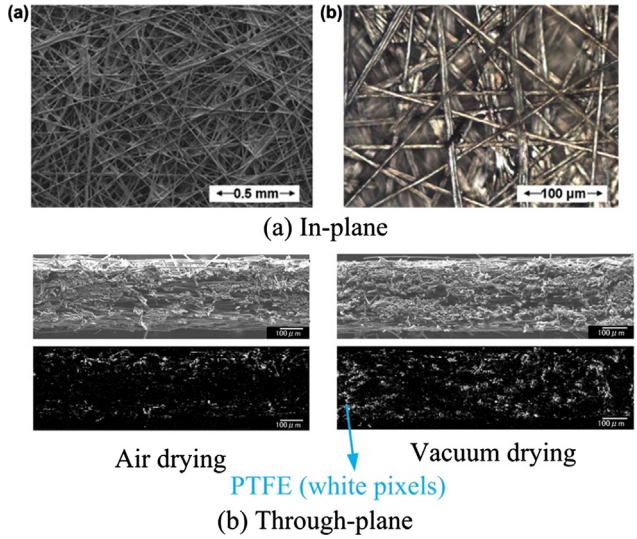

Fig. 1. Scanning electron microscopy (SEM) and energy dispersive X-ray spectroscopy (EDS) images of Toray-090 carbon paper. (a) In-plane [5] and (b) through-plane [20].

method to measure the P_c-s correlation under various GDL thickness, PTFE loading, and compression. They found water withdrawal occurs at a negative capillary pressure and observed hysteresis between water injection and withdrawal processes. Kumbur et al. [24] measured the P_c-s curves for SGL 24 series GDLs using the MSP technique. They derived a new K function to replace the J function in the standard Leverett correlation, which takes into account the PTFE loading (ranging from 5 wt% to 20 wt%). Hao and Cheng [26] developed a micro-fluidic device to investigate the P_c-s curves of the Toray-090 carbon paper coated with different PTFE loadings (10 wt% and 30 wt%). They determined the parameters in the Leverett J correlation using experimental data.

Numerical study is an efficient tool to investigate the complex two-phase transport in GDLs, such as the multiphase mixture (M2) model [27–31], two-fluid model [32], lattice Boltzmann method (LBM) [26,33–36], pore network method (PNM) [37–40] and volume of fluid

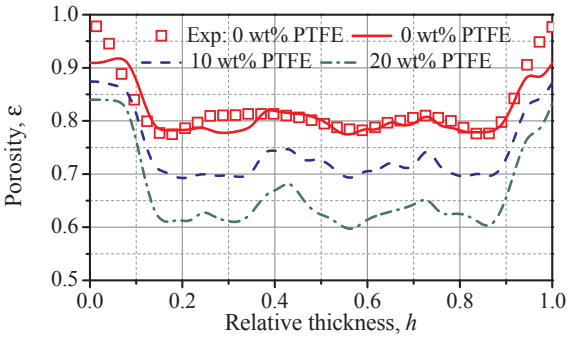

Fig. 3. Comparisons of simulated and experimental local porosity distribution [51] along the through-plane direction for GDLs.

(VOF) method [41–45]. Wang and Chen [27] compared their M^2 model prediction (based on the standard Leverett correlation) of the liquid water through-plane profile with the high-resolution neutron radiography data, and showed an acceptable agreement in the GDL regions. Wang and Chen [28] further explored the spatial variation in GDL properties including porosity, permeability, and wettability, and derived a generalized formula based on the standard Leverett correlation to account for the impacts of the property spatial variation. They also explained local water accumulation observed in high-resolution neutron radiography of GDLs and achieved a good agreement with the experimental water profile. The impact of land compression was also discussed and compared with experiment. Wu et al. [29] employed a M^2 model to explore how the arrangement pattern of the protrusive GDL affects the fuel cell performance. They found that the small density of protrusive GDL distribution can enhance the fuel flow into the catalyst layer with the smallest pressure drop. Si et al. [32] adopted a two-fluid model which incorporated a validated Leverett function (K function) in ref. [24] to investigate the effect of different PTFE loadings, compression pressure and micro-porous layer (MPL) on the cell performance. They found liquid water is hard to be removed from the GDL with poor hydrophobicity. Hao and Cheng [26] developed a three-dimensional (3D) LBM model to perform pore scale simulations of air-water flow in the mixed-wettability carbon paper GDL. They validated

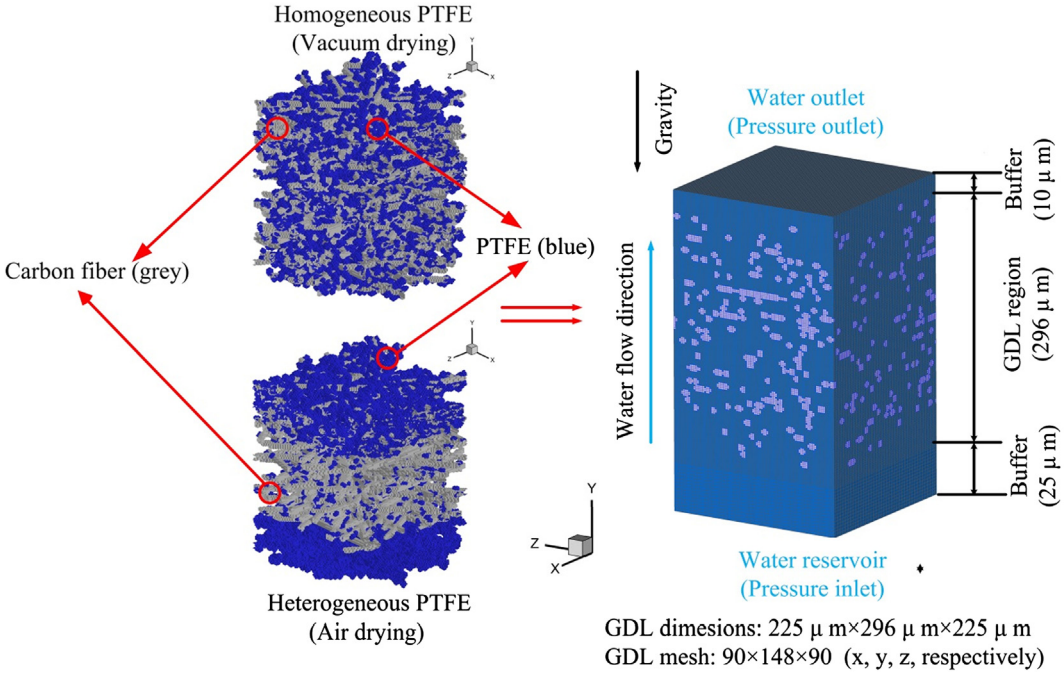

Fig. 2. Computational domain and boundary conditions of present two-phase GDL model.

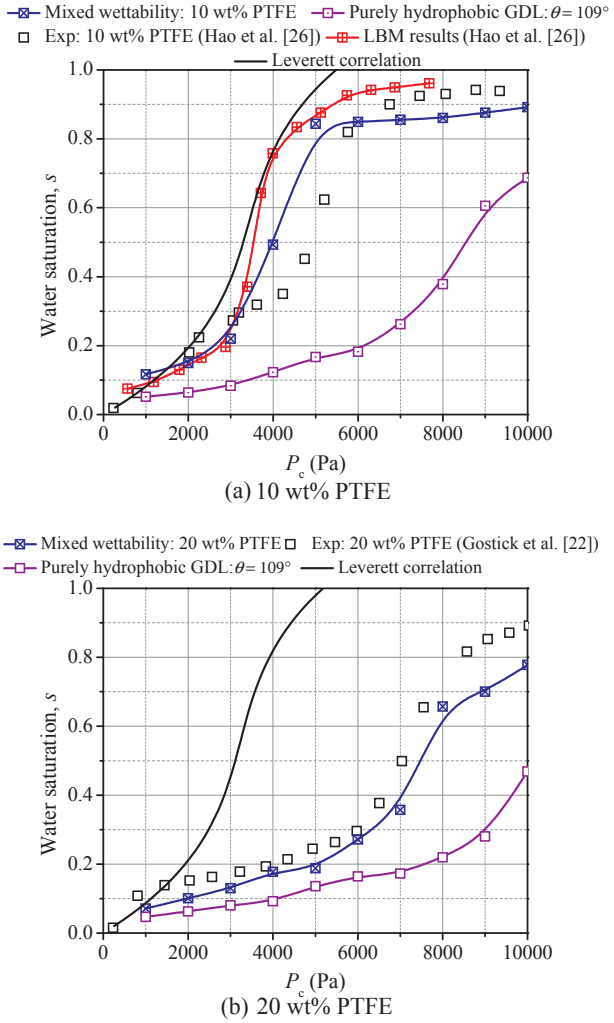

Fig. 4. Comparisons of P_c-s curves obtained from VOF simulations, LBM simulations [26] and experimental data [22,26] for GDLs with different PTFE loadings. Parameters for the Leverett J function model: Permeability $K = 4.24 \times 10^{-12}$, porosity $\varepsilon = 0.74$ (10 wt% PTFE) and 0.66 (20 wt% PTFE), contact angle $\theta = 109°$.

the simulated P_c-s curves with experimental data and further fitted capillary pressure data to obtain the proper parameters for the modified Leverett J function. Fang et al. [34] employed a multiple-relaxation-time LBM model to predict the effective transport properties of reconstructed perforated GDLs. They fitted effective transport properties of partially saturated GDL as correlations. Chen et al. [36] adopted a 3D multiphase LBM model to study the impact of PTFE loading and distribution on the air-water transport and gas relative permeability in GDL. They found that the simulated liquid water saturation in GDL decreases with the increase of PTFE loading in GDL. Sinha and Wang [37] developed a PNM model to investigate the impact of wettability distribution on flooding in GDL. They found liquid water preferentially flows through a connected hydrophilic pore network in a mixed-wettability GDL. Straubhaar et al. [38] developed a condensation PN model to investigate the formation of liquid water by condensation in GDL. Their numerical results agree well with several experimental data. Yin et al. [43] employed a two-phase VOF model to study the effect of the heterogeneous fiber contact angle on water transport in GDL. Niu et al. [44] employed the VOF method to investigate the liquid water removal via the by-pass flow under various wettability of GDLs and found that the corner droplet in the flow channel is easier to be removed by by-pass flow under the rib. Niu et al. [45] further extended the VOF study to investigate the through-plane water profiles by accounting for the

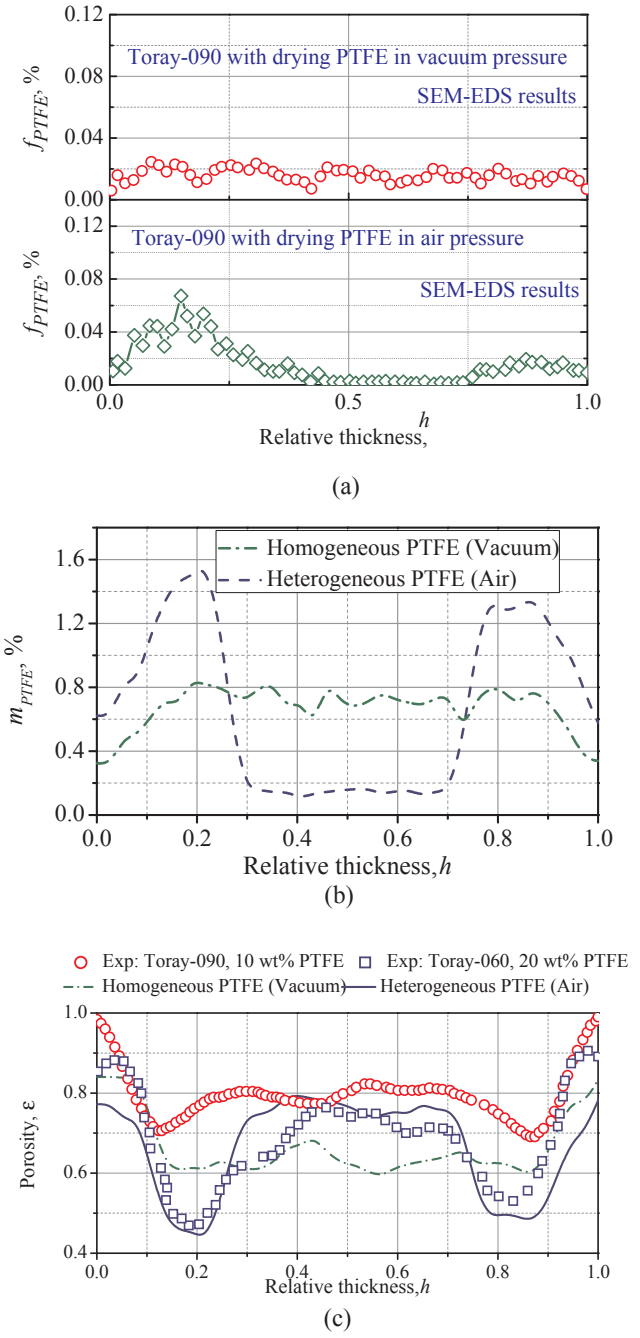

Fig. 5. Comparison of simulated and experimental local PTFE and porosity distribution along the through-plane direction for GDLs under different PTFE drying conditions (air pressure and vacuum pressure). (a) Experimental PTFE profiles in Ref. [20]; (b) simulated PTFE profiles in VOF model; (c) simulated local porosity profiles in VOF model and experimental porosity profiles in Refs. [51,52].

porosity spatial distribution determined by experiment. Good agreement was achieved for the liquid water through-plane profile under low pressure and the average saturation-capillary pressure correlation. The standard Leverett correlation was found to deviate from both the experimental and VOF prediction data under high pressure.

Though several numerical studies have been performed to study two-phase flow in GDLs, few were focused on the impacts of PTFE loadings and distributions in a mixed-wettability GDL [26,36]. One major reason is that those detailed PTFE distributions were only available recently when high-resolution scanning electron microscopy

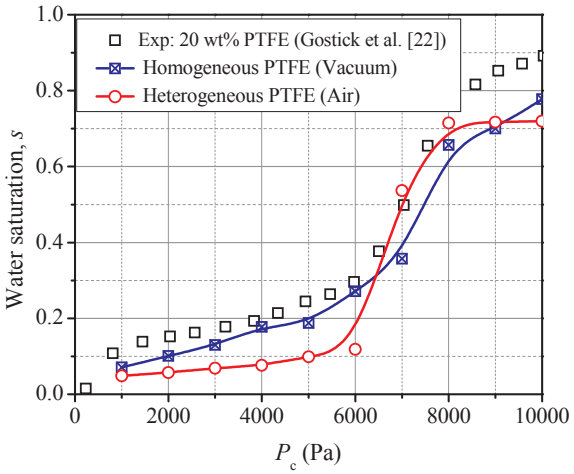

Fig. 6. Comparisons of P_c-s curves obtained from GDLs with different PTFE distributions.

(SEM) and energy dispersive X-ray spectroscopy (EDS) techniques were introduced to GDL studies. In this study, a 3D two-phase VOF model, along with a stochastic model of PTFE treated GDL microstructures reconstruction, was developed to investigate the P_c-s curves inside the Toray carbon paper GDL (TGP-090) with various PTFE loadings and spatial distributions. The simulated results were compared with the experimental data [22,26] and LBM results [26], as well as the standard Leverett J correlation. Summarily, the main objectives of this study are to develop a two-phase VOF model to simulate the air–water flow in GDLs with different PTFE treatments and PTFE local distributions, and to highlight the significant effects of mixed wettability on the P_c-s correlation of GDLs.

2. Model development

2.1. VOF model

(a) Governing equations

In the two-phase VOF model, the liquid water phase fraction γ is introduced as a main variable to be solved. The cells fully occupied by liquid water are marked as $\gamma = 1$, whereas cells fully occupied by air are marked as $\gamma = 0$. The cells with phase fraction between 0 and 1 consist of air-water interface. The volume averaged density and dynamic viscosity for air-water mixture, ρandμ, are calculated as follows:

$$\rho = \rho_l\gamma + \rho_g(1-\gamma) \tag{1}$$

$$\mu = \mu_l\gamma + \mu_g(1-\gamma) \tag{2}$$

where subscripts l and g denote the liquid phase and gas phase respectively.

The governing equations for the two-phase VOF model in this study are listed as follows [45]:

Continuity equation:

$$\nabla\cdot\vec{U} = 0 \tag{3}$$

Phase conservation equation:

$$\frac{\partial\gamma}{\partial t} + \nabla\cdot(\vec{U}\gamma) + \nabla\cdot[\vec{U}_r\gamma(1-\gamma)] = 0 \tag{4}$$

Momentum equation [46,47]:

$$\frac{\partial(\rho\vec{U})}{\partial t} + \nabla\cdot(\rho\vec{U}\vec{U}) - \nabla\cdot(\mu\nabla\vec{U}) - (\nabla\vec{U})\cdot\nabla\mu = -\nabla p_d - \vec{g}\cdot\vec{x}\nabla\rho + \sigma\kappa\nabla\gamma \tag{5}$$

where $\vec{U}$ is the effective velocity vector shared by the two phases throughout the flow domain, which is defined as

$$\vec{U} = \gamma\vec{U}_l + (1-\gamma)\vec{U}_g \tag{6}$$

$\vec{U}_r = \vec{U}_l - \vec{U}_g$ is the relative velocity of liquid and gas at the interface, designated as "compression velocity", the subscript r here denotes "relative velocity"; γ, σ andκ are the phase fraction, surface tension coefficient and mean curvature of the phase interface, respectively. p_d is a modified pressure for simplifying the boundary conditions, defined as

$$p_d = p - \rho\vec{g}\cdot\vec{x} \tag{7}$$

where $\vec{x}$ is the position vector and $\vec{g}$ is the gravity vector, the subscript d denotes "dynamic". In this VOF model, the continuum surface force (CSF) model is adopted to account for the effects of surface tension at the liquid-gas interface by adding a force source f_σ to Eq. (5), which is defined as follow

$$f_\sigma = \sigma\kappa\nabla\gamma \tag{8}$$

the subscript σ denotes "surface tension", where the mean curvature of the phase interface $\kappa$is determined by:

$$\kappa = -\nabla\cdot\vec{n} = -\nabla\cdot\left(\frac{\nabla\gamma}{|\nabla\gamma|}\right) \tag{9}$$

It can be observed that κ is the interface curvature that is calculated with the divergence of the unit interface normal $\vec{n}$ and the unit interface normal $\vec{n}$ can be approximated with $\nabla\gamma/|\nabla\gamma|$. The surface unit normal $\vec{n}$ is adjusted in the cells adjacent to the wall according to the following equation:

$$\vec{n} = \vec{n}_w\cos\theta + \vec{t}_w\sin\theta \tag{10}$$

where $\vec{n}_w$ is the unit vector normal to the wall, $\vec{t}_w$ is the unit vector tangential to the wall, the subscript w denotes wall. θ is the contact angle. In this study, only the constant contact angle is considered.

(b) Initial and boundary conditions

The GDL sample (Toray-090 carbon paper) in this study is 296 μm thick with a cross-section of 225 μm × 225 μm, which is same as values in Ref. [26]. Simulations were performed by imposing different inlet pressures of liquid water, while keeping the same outlet pressure. The liquid water saturation at different capillary pressure was obtained by increasing the inlet pressure gradually. The other side walls are assumed symmetric planes. The contact angle θ is set as 80° for carbon fiber and 109° for PTFE [7–9,48–50]. Initially, there was no liquid water in the GDL.

(c) Numerical procedures

The open source software Open FOAM was adopted to perform all the numerical simulations, and the semi-implicit method for pressure linked equation (SIMPLE) scheme was responsible for the coupling solution of the pressure and velocity. The computational domain of the present GDL was discretized with about 1 million of hexahedral mesh (90 × 148 × 90, x, y, z respectively), as shown in Fig. 2. The open-MPI was adopted for parallel computation. The time step was set 4×10^{-7} s. Each case took about 16 h by using 48 Intel Xeon @2.93 GHz processors in parallel. We used the hexahedral mesh for pore regions of GDLs, following our previous work [45] and other studies [26,33–36,43–45]. The chosen mesh size (2.5 μm) is similar to the LBM study in Ref. [26], our pervious validation work [45], and other VOF GDL simulations [43]. We also conducted a grid-independence study using a small domain, showing the approximation is accurate in predicting two-phase flow in GDLs using the chosen grid size. The fiber surface is treated as no-slip wall. The Reynolds number in the present

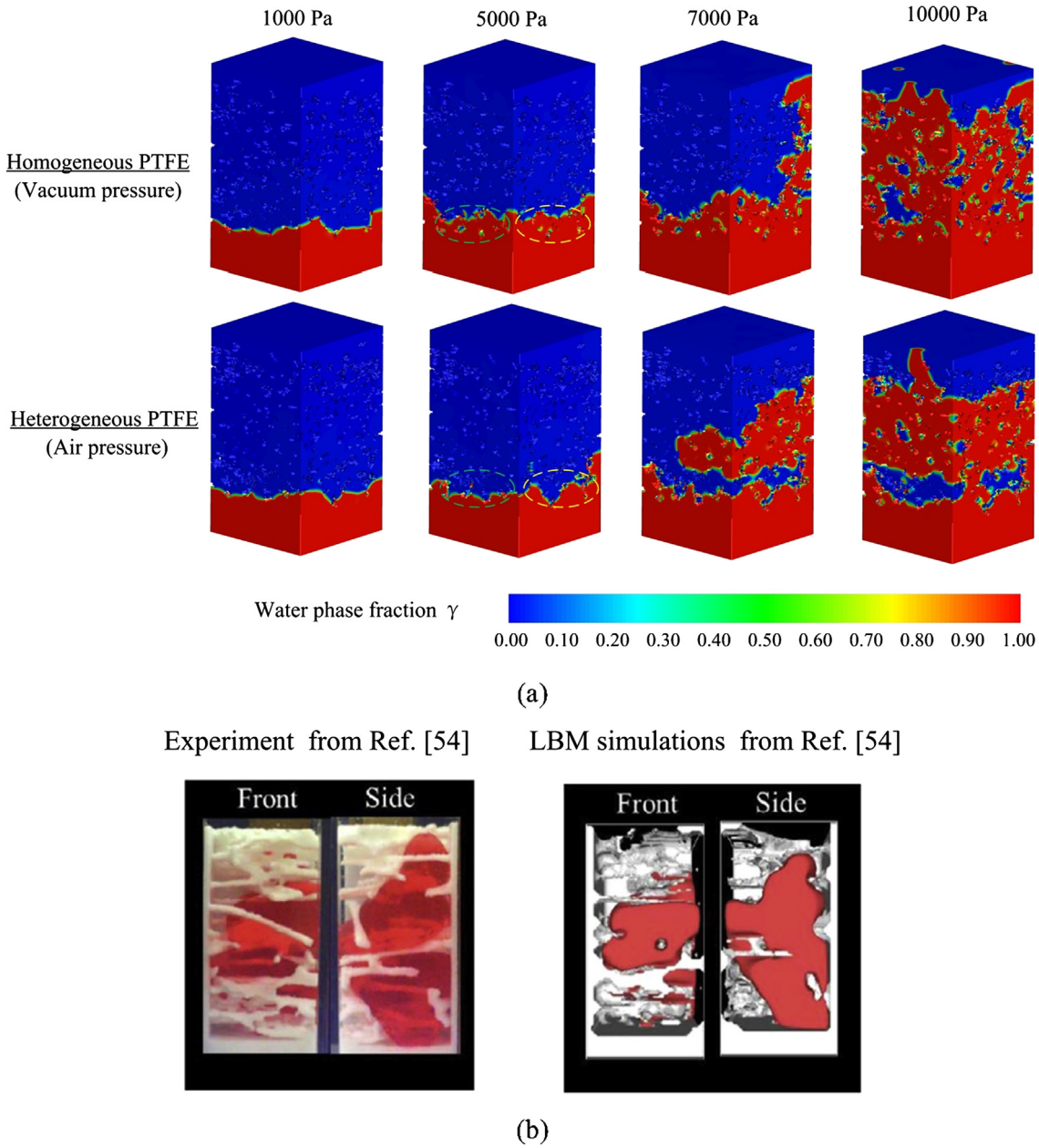

Fig. 7. Qualitative comparison among present VOF results, LBM simulations and experimental images. (a) Liquid water dynamics under different capillary pressure P_c for GDLs with different PTFE distributions; (b) experimental visualization and LBM simulations of liquid water dynamics in an enlarged GDL [54].

GDL ranges from about 0.01 to 0.1 based on the averaged water velocity (e.g. 0.011 m s^{-1}) at the inlet and fiber diameter 8 μm as the characteristic length. The flow recirculation behind fibers would be captured by this model if it physically occurs.

2.2. Stochastic model

Toray carbon paper consists of numerous horizontally orientated straight fibers, the scanning SEM and EDS images of Toray-090 in both directions of in-plane and through-plane are shown in Fig. 1. The Toray carbon paper TGP-090 was digitally reconstructed using a stochastic method [26,34,36,43–45]. Based on the GDL reconstruction method in our previous study [45], the Toray-090 carbon paper without PTFE treatment is firstly reconstructed (porosity $\varepsilon = 0.74$) and the fiber diameter is set as 8 μm. After generating fiber structures of the GDL without PTFE (Toray-090 0 wt% PTFE), the PTFE is added by randomly marking cells near the fiber surface as PTFE locations. This process was repeated until the target PTFE loading was achieved. This method of adding PTFE is similar with that in [26]. And the size of single PTFE parcel equals to the cell size. The PTFE with flake shape at the fiber intersection is also determined by this random process. The reconstructed fiber structures and PTFE locations (including both air and vacuum dryings) of Toray-090 are shown in Fig. 2. The distributions of simulated local porosity along the through-plane direction for GDLs with different PTFE loadings (0 wt%, 10 wt%, 20 wt%) were compared with experimental profiles in Ref. [51], as shown in Fig. 3.

3. Results and discussion

3.1. Effects of PTFE loading on liquid water transport

This section presents the effects of PTFE loadings on the liquid water transport in GDLs. The simulated P_c-s curves of GDLs with 10 wt% and 20 wt% PTFE loading were compared with experimental data in Ref.

[22,26] and LBM results in ref. [26]. Fig. 4a compared the simulated P_c-s curves with experimental data and LBM results for the GDL treated with 10 wt% PTFE [26]. It can be seen that the water saturation increases gradually as P_c under 3000 Pa. Then, a rapid increase of the water saturation was indicated when P_c raises over 3000 Pa. This rapid increase in the water saturation corresponds to liquid water breaking through the GDL. In the high capillary pressure region ($P_c > 5000$ Pa), the water saturation shows minor increment as P_c continues to increase. In overall, the numerical results agree well with experimental data. The LBM results for the GDL with 10 wt% PTFE are also plotted in Fig. 4a. It can be seen that the VOF prediction agrees with LBM results at the low P_c region but underestimates water saturation in the high P_c region. A purely hydrophobic GDL was also simulated for comparison, which deviates from the mixed-wettability GDL. Fig. 4b compares the simulated P_c-s curves with experimental data for the GDL of 20 wt% PTFE [22]. It can be seen that water breakthrough starts when P_c raises over 6000 Pa. The difference in the P_c-s curves between the purely hydrophobic and mixed-wettability GDLs decreases as PTFE loading increases. This may be due to the fact that the GDL of 20 wt% PTFE contains more hydrophobic pores.

Furthermore, the Leverett J correlation, a popular correlation for P_c-s in porous media, was compared with the simulated P_c-s curves of GDLs with different PTFE loadings, as shown in Fig. 4a and b. The Leverett J correlation is given below [26]:

$$P_c = \sigma\cos(\theta)\left(\frac{\varepsilon}{K}\right)^{1/2} J(s) \tag{11}$$

where ε and K are the average porosity and absolute permeability of the GDL, respectively. The standard Leverett function $J(s)$ for purely hydrophobic and hydrophilic porous media is following [26]:

$$J(s) = \begin{cases} -1.417(1-s) + 2.120(1-s)^2 - 1.263(1-s)^3, & \text{if } \theta > 90^\circ \text{ hydrophobic} \\ 1.417(1-s) - 2.120s^2 + 1.263s^3, & \text{if } \theta < 90^\circ \text{ hydrophilic} \end{cases} \tag{12}$$

It is seen in Fig. 4 that the simulated P_c-s curve is close to the Leverett correlation in the GDL with low PTFE loading (10 wt%), but deviates for high PTFE loading (20 wt%). Note that the Leverett J function was originally developed for homogeneous sand structures, which are different from the fibrous GDLs. Besides, the contact angle is assumed uniform in the Leverett J function, while PTFE treated GDLs show mixed wettability. Compared with the purely hydrophobic GDL, the mixed-wettability GDL model gives a P_c-s correlation closer to the experimental data.

3.2. Effects of PTFE spatial distribution on two-phase flow

GDLs are commonly treated with a hydrophobic agent such as PTFE to increase the hydrophobicity. In the treatment, GDLs are dipped into an aqueous PTFE dispersion to enable PTFE addition. Excess dispersion is allowed to dip off, then the remaining solvent is removed by oven drying. Finally, the PTFE is sintered at above 350 °C. In the PTFE drying process, e.g. the vacuum pressure (vacuum-dried) and atmospheric pressure (air-dried), have a significant impact on the PTFE distribution in the through-plane direction [20]. Fig. 1b shows the through-plane SEM images and corresponding EDS maps of PTFE distributions for GDLs with drying PTFE under air pressure (air drying) and vacuum pressure (vacuum drying) [20]. It is seen that PTFE is heterogeneously distributed near the top and bottom surface in the air drying GDL, whereas PTFE is distributed more homogeneously through the bulk under the vacuum drying condition. The cause is the absence of capillary force in the vacuum pressure condition, which enables the PTFE solution to permeate GDL deeply. The experimentally measured PTFE distributions f_{PTFE} along the through-plane direction for GDLs with two PTFE drying methods [20] are shown in Fig. 5a. The grey-scale of each pixel along the in-plane direction of the EDS image in Fig. 1b was summed to obtain a relative PTFE value. After that, the relative PTFE values were normalized across the through-plane direction to obtain f_{PTFE}.

In this section, two kinds of PTFE distributions were investigated for the two drying methods [20], as shown in Fig. 5a. It is noted that this study considers effects of different drying methods by mapping the experimentally determined PTFE profiles of two drying methods in [20] to the present GDL. The physical PTFE drying process is interesting, but out of scope of this model, thus was excluded in this study. Both GDLs were treated with 20 wt% PTFE in the GDL reconstruction and VOF simulation. The profiles of the corresponding m_{PTFE} are shown in Fig. 5b. m_{PTFE} is defined as the total mass of local PTFE in the in-plane direction divided by the sum of PTFE in the entire GDL. Because the PTFE is physically present in the pore network, its addition will reduce local porosity [51]. The local porosity profiles used in the VOF simulation are given in Fig. 5c. Because of the more PTFE loading near the top and bottom surface, two dense layers occur in the GDL with air drying PTFE.

Fig. 6 shows the simulated P_c-s curves for the GDLs under air and vacuum drying methods, respectively. It can be seen that water saturation of the GDL with air drying PTFE is lower than that of the GDL with vacuum drying GDL in the low P_c region ($P_c < 6000$ Pa). The reason may be due to the low local porosity near the inlet, caused by the more PTFE loading. Besides, the maximum of the water saturation in the GDL with air drying PTFE is larger than that in the GDL with vacuum drying when water breakthrough starts.

Fig. 7a shows the liquid water dynamics (characterized by the value of water phase fraction $\gamma = 1$) in GDLs with the two PTFE drying methods, respectively. Both GDLs have similar water dynamics when P_c is low. Slight difference is present in local, as highlighted by the dash circles. Under the high P_c of 7000 and 10,000 Pa, a barrier to water imbibition for air drying can be observed (the blue or water-free zone in the lower side), which blocks water breakthrough. For 7000 Pa, when liquid water starts to break through the GDL with air drying PTFE, it firstly fills the middle region. In comparison, liquid breaks through the vacuum drying GDL directly, as shown in Fig. 7a. The reason for this significant difference is that a higher PTFE concentration appears near the water inlet in the air drying GDL, which presents a large barrier for water imbibition. In addition, the middle region has low PTFE loading for air drying PTFE, which permits liquid to occupy the region after overcoming the first barrier. Wang and Chen [27] showed water local accumulation in the middle of GDLs in both their model prediction and neutron radiography data. In addition, fluctuation in the local water content may arise from spatial variation in porosity and permeability [28], phase change [53], and liquid water cross-flow under ribs [44]. In our previous study [45] that used a similar model, we have compared the predicted liquid water dynamics in GDLs with experimental data obtained by the X-ray tomographic microscopy (XTM) for constant-contact-angle GDLs. Moreover, the present study already compares the predicted liquid dynamics in Fig. 7a qualitatively with both experimental data and LBM simulations [54] under the similar GDL configurations, as shown in Fig. 7b.

4. Conclusions

In this study, the air-water two-phase flow in the mixed-wettability gas diffusion layer (GDL) was investigated using a three-dimensional (3D) volume of fluid (VOF) model. A stochastic method was developed to reconstruct the microstructures of mixed-wettability GDLs with different PTFE loadings.

(1) The VOF model predictions were validated with experimental data and lattice Boltzmann method (LBM) results. The predicted curves of the capillary pressure P_c versus water saturation s, i.e. P_c-s, agreed well with the experimental data, and were slightly lower

than the LBM results.

(2) Two PTFE spatial distributions caused by two PTFE drying methods, i.e. air pressure and vacuum pressure, respectively, were investigated. The air drying GDL requires a higher breakthrough pressure.
(3) The model prediction of the P_c-s curves was compared with the Leverett J correlation. It was found that the two were close under the lower PTFE loadings (10 wt%), but large deviation was presented under the higher loading (20 wt%).
(4) Comparing with the purely hydrophobic GDL case, the mixed-wettability GDL showed a P_c-s curve more close to experimental data, indicating that the mixed wettability in the PTFE treated GDL needs to be taken into account in order to accurately predict two-phase behaviors.

Overall, the present study highlights the significant effects of PTFE distributions caused by the different drying methods in real applications. The developed two-phase VOF GDL model benefits the accurate prediction of correlation of capillary pressure and water saturation in the mixed-wettability gas diffusion layers. In addition, practical GDLs can be fabricated with a PTFE loading spatial variation using either different drying methods or other coating methods to improve water management. The proposed VOF model provides a fast and efficient tool to optimize the loading variation for water management purpose.

Acknowledgement

This work is supported by the National Natural Science Foundation of China for Excellent Young Scholars (Grant No. 51622606), and the Key Program of Natural Science Foundation of Tianjin (China) (Grant No. 16JCZDJC30800). Y. Wang and J. Wu also thank Shanghai Everpower Technologies Ltd for partial financial support.

References

[1] Wang Y, Chen KS, Mishler J, Cho SC, Adroher XC. A review of polymer electrolyte membrane fuel cells: technology, applications, and needs on fundamental research. Appl Energy 2011;88:981–1007.
[2] Wu HW. A review of recent development: transport and performance modeling of PEM fuel cells. Appl Energy 2016;165:81–106.
[3] Wang Y, Chen K. PEM fuel cells: thermal and water management fundamentals. Momentum Press 2013. https://doi.org/10.5643/9781606502471.
[4] Jiao K, Li XG. Water transport in polymer electrolyte membrane fuel cells. Prog Energy Combust Sci 2011;37:221–91.
[5] Wang Y, Cho SC, Thiedmann R, Schmidt V, Lehnert W, Feng XH. Stochastic modeling and direct simulation of the diffusion media for polymer electrolyte fuel cells. Int J Heat Mass Transfer 2010;53:1128–38.
[6] Park J, Oh H, Lee Y, Min K, Lee E, Jyoung J. Effefct of the pore size variation in the substrate of the gas diffusion layer on water management and fuel cell performance. Appl Energy 2016;171:200–12.
[7] Adamson AW, Gast AP. The solid-liquid interface-contact angle. 6th ed. In: Physical chemistry of surfaces. New York: John Wiley & Sons Inc; 1967. p. 362–72.
[8] Mattia D, Bau HH, Gogotsi Y. Wetting of CVD carbon films by polar and nonpolar liquids and implications for carbon nanopipes. Langmuir 2006;22(4):1789–94.
[9] Wood DL, Rulison C, Borup RL. Surface properties of PEMFC gas diffusion layers. J Electrochem Soc. 2010;157(2):B195–206.
[10] Bevers D, Rogers R, Bradke MV. Examination of the influence of PTFE coating on the properties of carbon paper in polymer electrolyte fuel cells. J Power Sources 1996;63:193–201.
[11] Mathias M, Roth J, Fleming J, Lehnert W. Diffusion media materials and characterization. In: Lietsich W, Lamm A, Gasteiger HA, editors. Handbook of fuel cells-fundamentals, technology and applications. John Wiley & Sons, Ltd; 2003.
[12] Lin GY, Nguyen TV. Effect of thickness and hydrophobic polymer content of the Gas diffusion layer on electrode flooding level in a PEMFC. J Electrochem Soc 2005;152(10):1942–8.
[13] El-kharouf A, Mason TJ, Brett DJ, Pollet BG. Ex-situ characterisation of gas diffusion layers for proton exchange membrane fuel cells. J Power Sources 2012;218:393–404.
[14] Ismail MS, Hughes KJ, Ingham DB, Ma L, Pourkashanian M. Effect of PTFE loading of gas diffusion layers on the performance of proton exchange membrane fuel cells running at high-efficiency operating conditions. Int J Energy Res 2013;37:1592–9.
[15] Qiu DK, Janßen H, Peng LF, Irmscher P, Lai XM, Lehnert W. Electrical resistance and microstructure of typical gas diffusion layers for proton exchange membrane fuel cell under compression. Appl Energy 2018;231:127–37.
[16] Lee YT, Kim B, Kim YC, Li XG. Degradation of gas diffusion layers through repetitive freezing. Appl Energy 2011;88:5111–9.
[17] Ma R, Yang T, Breaz E, Li ZL, Briois P, Gao F. Data-driven proton exchange membrane fuel cell degradation prediction through deep learning method. Appl Energy 2018;231:102–15.
[18] Yu SC, Li XJ, Li J, Liu S, Lu WT, Shao ZG, et al. Study on hydrophobicity degradation of gas diffusion layer in proton exchange membrane fuel cells. Energy Convers Manage 2013;76:301–6.
[19] Park JM, Oh HY, Ha TH, Lee YI, Min KD. A review of the gas diffusion layer in proton exchange membrane fuel cells: durability and degradation. Appl Energy 2015;155:866–80.
[20] Ito H, Abe K, Ishida M, Nakano A, Maeda T, Munakata T, et al. Effect of through-plane distribution of polytetrafluoroethylene in carbon paper on in-plane gas permeability. J Power Sources 2014;248:822–30.
[21] Gostick JT, Fowler MW, Ioannidis MA, Pritzker MD, Volfkovich YM, Sakars A. Capillary pressure and hydrophilic porosity in gas diffusion layers for polymer electrolyte fuel cells. J Power Sources 2006;156:375–87.
[22] Gostick JT, Marios AI, Fowler MW, Pritzker MD. Wettability and capillary behavior of fibrous gas diffusion media for polymer electrolyte membrane fuel cells. J Power Sources 2009;194:433–44.
[23] Fairweather JD, Cheung P, St-Pierre J, Schwartz DT. A microfluidic approach for measuring capillary pressure in PEMFC gas diffusion layers. Electrochem Commun 2007;9:2340–5.
[24] Kumbur EC, Sharp KV, Mench MM. Validated Leverett approach for multiphase flow in PEFC diffusion media I. Hydrophobicity effect. J Electrochem Soc 2007;154:B1295–304.
[25] Nguyen TV, Lin G, Ohn H, Wang X. Measurement of capillary pressure property of gas diffusion media used in proton exchange membrane fuel cells. Electrochem Solid-State Lett 2008;11:B127–31.
[26] Hao L, Cheng P. Capillary pressures in carbon paper gas diffusion layers having hydrophilic and hydrophobic pores. Int J Heat and Mass Transfer 2012;55:133–9.
[27] Wang Y, Chen KS. Through-plane water distribution in a polymer electrolyte fuel cell: comparison of numerical prediction with neutron radiography data. J Electrochem Soc 2010;157:B1879–86.
[28] Wang Y, Chen KS. Effect of spatially-varying GDL properties and land compression on water distribution in PEM fuel cells. J Electrochem Soc 2011;158:B1292–9.
[29] Wu HW, Shih GJ, Chen YB. Effect of operational parameters on transport and performance of a PEM fuel cell with the best protrusive gas diffusion layer arrangement. Appl Energy 2018;220:47–58.
[30] Zamel N, Li XG. A parametric study of multi-phase and multi-species transport in the cathode of PEM fuel cells. Int J Energy Research 2008;32:698–721.
[31] Wang Y. Modeling of two-phase transport in the diffusion media of polymer electrolyte fuel cells. J Power Sources 2008;185:261–71.
[32] Si C, Lu G, Wang XD, Lee DJ. Gas diffusion layer properties on the performance of proton exchange membrane fuel cell: p_c-s relationship with K-function. Int J Hydrogen Energy 2016;41:21827–37.
[33] Jinuntuya F, Whiteley M, Chen R, Fly A. The effects of gas diffusion layers structure on water transportation using X-ray computed tomography based Lattice Boltzmann method. J Power Sources 2018;378:53–65.
[34] Fang WZ, Tang YQ, Chen L, Kang QJ, Tao WQ. Influence of the perforation on effective transport properties of gas diffusion layers. Int J Heat and Mass Transfer 2018;126:243–55.
[35] Molaeimanesh GR, Akbari MH. Impact of PTFE distribution on the removal of liquid water from a PEMFC electrode by lattice Boltzmann method. Int J Hydrogen Energy 2014;39:8401–9.
[36] Chen W, Jiang FM. Impact of PTFE content and distribution on liquid–gas flow in PEMFC carbon paper gas distribution layer: 3D lattice Boltzmann simulations. Int J Hydrogen Energy 2016;41:8550–62.
[37] Sinha PK, Wang CY. Liquid water transport in a mixed-wet gas diffusion layer of a polymer electrolyte fuel cell. Chem Eng Sci 2008;63:1081–91.
[38] Straubhaar B, Pauchet J, Prat M. Pore network modeling of condensation in gas diffusion layers of proton exchange membrane fuel cells. Int J Heat and Mass Transfer 2016;102:891–901.
[39] Shahraeeni M, Hoorfar M. Pore-network modeling of liquid water flow in gas diffusion layers of proton exchange membrane fuel cells. Int J Hydrogen Energy 2014;39:10697–709.
[40] Agaesse T, Lamibrac A, Büchi FN, Pauchet J, Prat M. Validation of pore network simulations of ex-situ water distributions in a gas diffusion layer of proton exchange membrane fuel cells with X-ray tomographic images. J Power Sources 2016;331:462–74.
[41] Park JW, Jiao K, Li XG. Numerical investigations on liquid water removal from the porous gas diffusion layer by reactant flow. Appl Energy 2010;87:2180–6.
[42] Ferreira RB, Falcao DS, Oliveria VB, Pinto AM. 1D + 3D two-phase flow numerical model of a proton exchange membrane fuel cell. Appl Energy 2017;203:474–95.
[43] Yin Y, Wu TT, He P, Du Q, Jiao K. Numerical simulation of two-phase cross flow in microstructure of gas diffusion layer with variable contact angle. Int J Hydrogen Energy 2014;39:15772–85.
[44] Niu ZQ, Jiao K, Wang Y, Du Q, Yin Y. Numerical simulation of two-phase cross flow in the gas diffusion layer microstructure of proton exchange membrane fuel cells. Int J Energy Research 2018;42:802–16.
[45] Niu ZQ, Wang Y, Jiao K, Wu JT. Two-Phase flow dynamics in the gas diffusion layer of proton exchange membrane fuel cells: volume of fluid modeling and comparison with experiment. J Electrochem Soc 2018;165(9):F613–20.
[46] Deshpande SS, Anumolu L, Trujillo MF. Evaluating the performance of the two-phase flow solver interFoam. Comput Sci Discov 2012;5(1):014016.
[47] Berberovic E, Hinsberg NP, Jakirlic S, Roisman IV, Tropea C. Drop impact onto a liquid layer of finite thickness: dynamics of the cavity evolution. Phys Rev E

2009;79:036306.
[48] Goswami S, Klaus S, Benziger J. Wetting and absorption of water drops on Nafion films. Langmuir 2008;24:8627–33.
[49] Bernett MK, Zisman WA. Relation of wettability by aqueous solutions to the surface constitution of low-energy solids. J Phys Chem 1959;63:1241–6.
[50] Zhang JL, Li J, Han YC. Superhydrophobic PTFE surfaces by extension. Macromol Rapid Commun 2004;25:1105–8.
[51] Fishman Z, Bazylak A. Heterogeneous through-plane porosity distributions for treated PEMFC GDLs I. PTFE effect. J Electrochem Soc 2011;158:B841–5.
[52] Flückiger R, Marone F, Stampanoni M, Wokaun A, Büchi FN. Investigation of liquid water in gas diffusion layers of polymer electrolyte fuel cells using X-ray tomographic microscopy. Electrochimia Acta 2011;56:2254–62.
[53] Wang Y, Chen KS. Advanced control of liquid water region in diffusion media of polymer electrolyte fuel cells through a dimensionless number. J Power Sources 2016;315:224–35.
[54] Sakaida S, Tabe Y, Chikahisa T. Large scale simulation of liquid water transport in a gas diffusion layer of polymer electrolyte membrane fuel cells using the lattice Boltzmann method. J Power Sources 2017;361:133–43.